Physics Letters B 837 (2023) 137648

Contents lists available at ScienceDirect

Physics Letters B

journal homepage: www.elsevier.com/locate/physletb

Neutron and gamma multiplicities calculated in the consistent framework of the Hauser-Feshbach Monte Carlo code FIFRELIN

V. Piau [a], O. Litaize [a,*], A. Chebboubi [a], S. Oberstedt [b], A. Göök [c], A. Oberstedt [d]

[a] CEA/DES/IRESNE/DER/SPRC/LEPh, Cadarache, 13108 Saint-Paul lez Durance, France
[b] European Commission, Joint Research Centre (JRC), 2440 Geel, Belgium
[c] Department of Physics and Astronomy, Uppsala University, Box 516, 751 20 Uppsala, Sweden
[d] Extreme Light Infrastructure - Nuclear Physics (ELI-NP), Horia Hulubei National Institute for Physics and Nuclear Engineering (IFIN-HH), 077125 Bucharest-Magurele, Romania

ARTICLE INFO

Article history:
Received 5 July 2022
Received in revised form 19 December 2022
Accepted 23 December 2022
Available online 29 December 2022
Editor: J.-P. Blaizot

Keywords:
Nuclear fission
γ-ray multiplicity
Monte Carlo
Fragment de-excitation
Nuclear level densities

ABSTRACT

Monte-Carlo simulations to calculate the number of prompt particles emitted during fission were performed using the FIFRELIN code and compared to recent experimental data. We show that we are able to reproduce both the neutron and γ-ray multiplicity distributions as a function of the pre-neutron mass of the fission fragments using a single consistent set of parameters. This result was made possible by using an energy-dependent spin cut-off model, driving the initial total angular momentum of the fission fragments, together with microscopic level densities from the HFB plus combinatorial method. We also discuss, how the initial excitation-energy sharing shapes the TKE-dependent γ-ray multiplicity.

1. Introduction

Nuclear fission is a complex process that proceeds after scission via the de-excitation of neutron-rich primary fragments to fission products. During this de-excitation, various prompt and delayed particles (neutrons, photons and electrons) are emitted. To better understand this process, modeling codes such as FIFRELIN [1] are developed, which aim at reproducing and predicting fission observables, e.g., prompt neutron and γ-ray multiplicities, $\bar{\nu}$ and $\bar{M}_\gamma$, using nuclear models. As already stated in Ref. [2], such observables measured in correlation with fragment properties, e.g., mass (A) and total kinetic energy (TKE), are of particular interest, because they are more suitable than average characteristics to benchmark nuclear models and to constrain their parameters. At JRC-Geel, the VESPA setup [3] was designed to measure these correlated prompt fission observables.

Since the FIFRELIN code is based on a Hauser-Feshbach Monte Carlo approach, implementing the notion of nuclear realizations, we are able to estimate any fission observable in correlation with any other observable or parameter such as mass (A), charge (Z) and kinetic energy (KE) of the Fission Fragments (FFs). In this framework, it has been quite difficult to reproduce both $\bar{\nu}(A)$ and $\bar{M}_\gamma(A)$ within one consistent calculation. This was due to compensating model defects arising from different steps: estimation of excitation energy, sampling of the total angular momentum and parity of the two complementary fragments, realization of the corresponding nuclear level schemes, estimation of neutron/γ transmission coefficients and estimation of the internal conversion electron component. Here, we show that the use of an energy-dependent spin cut-off and a Hartree-Fock-Bogoliubov (HFB) microscopic level density model, based on a Skyrme effective interaction, allows us to reproduce both $\bar{\nu}(A)$ and $\bar{M}_\gamma(A)$ with an excellent agreement.

2. The experimental setup

The data that is compared in this work with our calculations was obtained from the spontaneous fission of ^{252}Cf with the VErsatile γ SPectrometer Array (VESPA) [3]. The spectrometer consists of several $LaBr_3(Ce)$ scintillators for γ-ray spectroscopy and was coupled with a position-sensitive twin Frisch-grid ionization chamber (IC), developed at JRC-Geel [4]. Fission fragment mass and total kinetic energy (TKE) are extracted using the double-kinetic energy ($2E$) method, as described in [5–7]. Fission fragment characteristics were obtained using the $\bar{\nu}(A)$ distribution reported in Ref. [5]. The post-neutron mass resolution (FWHM) of the IC is around 5 u [3]. The ionization chamber was calibrated to repro-

* Corresponding author.
E-mail address: olivier.litaize@cea.fr (O. Litaize).

https://doi.org/10.1016/j.physletb.2022.137648

duce the recommended average pre-neutron TKE from Ref. [8], that is $\langle \mathrm{TKE} \rangle = (184.1 \pm 1.3)$ MeV.

Combining the fission fragment characteristics with γ-ray data from the scintillation detectors makes it possible to measure multiple fission observables and their correlations. The superior energy and excellent timing resolution of the $LaBr_3(Ce)$ detectors allowed discriminating the prompt γ-peak from the isomeric transitions and γ rays from inelastic scattering of prompt fission neutrons in the detector material [9].

The VESPA setup has been used to extract the mass- and TKE-dependent prompt γ-ray multiplicity. The method used to extract these distributions is based on the Doppler aberration caused by the moving fragments, which creates an anisotropy of the prompt γ-ray emission in the laboratory frame [10,11]. The analysis procedure of the VESPA data with respect to this method is detailed in Ref. [3].

3. The FIFRELIN code

3.1. Overview

FIFRELIN [1] is a Monte-Carlo code developed by the CEA which simulates the de-excitation of nuclei. It can be used to calculate either the simple de-excitation of a single nucleus from a well-defined excited state, see e.g., Ref. [12], or complete fission events. The latter is the case that will be discussed in the following. It requires an additional step compared to a simple de-excitation, i.e., the sampling of the primary FF characteristics. In FIFRELIN, only binary fission is considered, and the emission of ternary particles is neglected. The mass and kinetic energy of each fragment are sampled from input distributions. Here we used the two-dimensional experimental yield $Y(A, \mathrm{TKE})$ from the VESPA experiment. Then, the charge of the fragments is derived from the Wahl model [13]. As FFs are left in an excited state, it is also necessary to determine their initial excitation energy E, angular momentum J and parity π. Then, the prompt de-excitation of the primary fragments is modeled in a Hauser-Feshbach framework [14] using the nuclear realization algorithm [15,16]. The fission observables obtained with FIFRELIN are the quantities related to this prompt emission, namely the fission products and prompt particles characteristics. The delayed components from the β decay of the fission products are not included in the simulation.

3.2. Excited states of fission fragments

In FIFRELIN, the excitation energy of a primary fragment is separated into the rotational energy, E_{rot}, and the intrinsic excitation energy, E^*_{int}. The rotational energy depends on the angular momentum of the fragment, and a Fermi-gas relation is assumed for the intrinsic excitation energy:

$$E^*_{\mathrm{int}} = aT^2 \,, \tag{1}$$

where $a(E, Z, A)$ is the energy-dependent level density parameter, following Ignatyuk's prescription [17,18]. Following Eq. (1), the intrinsic excitation energy is shared between the two fission fragments using a temperature-ratio parameterization ($R_T = T_L/T_H$) depicted in Fig. 1. Then, the energy of the heavy fragment is for instance given by:

$$E^*_H = \frac{\mathrm{TXE} - E_{\mathrm{rot},L} - E_{\mathrm{rot},H}}{1 + \dfrac{a_L}{a_H} R_T^2} \,, \tag{2}$$

where TXE is the total excitation energy. More details about this procedure can be found in Refs. [1,19,20].

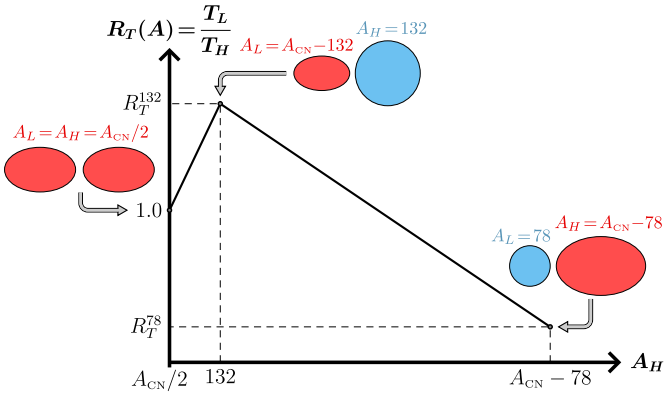

Fig. 1. Temperature-ratio parameterization $R_T(A)$.

The angular momentum of each fragment is sampled from the following distribution:

$$P(J) = \frac{2J+1}{2\sigma^2} \exp\left(\frac{-(J+1/2)^2}{2\sigma^2} \right) \,, \tag{3}$$

where σ^2 is called the spin cut-off parameter, that drives the dispersion and the mean value of the distribution: $\langle J \rangle \simeq \sigma\sqrt{\pi/2} - 1/2$. In this process, the angular momenta of the two fission fragments are sampled independently. Several models were tested in FIFRELIN [21], but we will only focus on two of them, also described and compared in Ref. [20]. The first and simplest model is the *Constant model* (CST), where constant spin cut-off values are selected for the light (L) and heavy (H) fragments:

$$\sigma^2_{L,H} = \begin{cases} k_L^2 \,, & A \leq A_{\mathrm{CN}}/2 \\ k_H^2 \,, & A > A_{\mathrm{CN}}/2 \end{cases} \,. \tag{4}$$

The second model will be referred to as the *Energy Dependent Spin cut-off model* (EDS). At high energy ($E > S_n$), this spin cut-off is based on the Fermi gas model, corrected for shell effects (see Ref. [18] and references therein):

$$\sigma^2_{\mathrm{EDS}}(A, Z, E \geq S_n) = f_\sigma^2 \times \mathcal{I}_0 \frac{a}{\tilde{a}} \sqrt{\frac{U}{a}} \,, \tag{5}$$

where $\mathcal{I}_0$ is the moment of inertia of a spheroid, which depends on the mass A and deformation β of the fragment. $U = E - \Delta$ denotes the excitation energy corrected for pairing effects, and $\tilde{a}(A)$ is the asymptotic value of the level density parameter $a(E, Z, A)$. This formula is applied to light (heavy) fragment by using the corresponding scaling factor f_{σ_L} (f_{σ_H}). At low energies, we follow the RIPL-3 recommendation [18, page 3147] and use the spin cut-off based on the spins of the known discrete levels of the associated fragment: $\sigma_d(A, Z)$. In both models, the parity of the fragment is sampled assuming parity equipartition.

In this process of generating the FF, four free parameters can be identified. The first two are the R_T^{132} and R_T^{78} values, parameterizing the excitation energy sharing as depicted in Fig. 1. The two others are related to the spin cut-off model chosen for the calculation. In the case of the CST spin cut-off model, the free parameters are the values k_L and k_H. For the EDS model, they are the two scaling factors f_{σ_L} and f_{σ_H}. The values of these parameters are chosen so that the associated FIFRELIN calculation reproduces the mean neutron multiplicities of the light and heavy fragments, $\bar{\nu}_L$ and $\bar{\nu}_H$ respectively. For the ^{252}Cf spontaneous fission, we use the multiplicities measured by Vorobyev *et al.* [22].

3.3. Coupled prompt de-excitation

After the procedure described above, each FF is fully characterized by an initial excited state $\mathcal{S}_i = \{A, Z, E, J, \pi\}$. Within the Hauser-Feshbach statistical model [14], the probability of reaching a final state $\mathcal{S}_f$ by emitting a particle p (neutron or photon) of energy ϵ_p and characterized by a set α of quantum numbers is given by:

$$P_p(\mathcal{S}_i \to \mathcal{S}_f, \alpha) = \frac{\Gamma_p(i \to f, \alpha)}{\Gamma_\gamma^{tot} + \Gamma_n^{tot}} , \tag{6}$$

where $\Gamma_p(i \to f, \alpha)$ is the partial width of the transition $\mathcal{S}_i \to \mathcal{S}_f$ [16,23]. The γ-ray emission is characterized by the type, X, (electric or magnetic) and the multipolarity, L, of the transition. The associated partial width is calculated from the photon strength function, f_{XL}. Neutron emission is only possible when $E > S_n$. In this case, the partial width of the transition is calculated from neutron transmission coefficients, which depend on the neutron orbital and total angular momenta, ℓ and j, respectively. Conversion electrons can also be emitted during the de-excitation process. The competition between γ emission and internal conversion is driven by the internal conversion coefficient (ICC). Compared to Ref. [1], conversion electron emission is now fully accounted for throughout the entire nuclear level scheme by tabulating internal conversion coefficients using the BrIcc code [24]. ICC values are calculated following the frozen orbital approximation from $Z = 10$ to 110, multipolarities $L = 1$ to 5, and shells K to P, including subshells. The energy range is $[E_{\text{shell}} + 1\,\text{keV},\ 6\,\text{MeV}]$, where E_{shell} is the electron binding energy of a given shell [25]. The possibility to emit an electron-positron pair is also taken into account.

FIFRELIN uses the Nuclear Realization (NR) formalism, introduced by Bečvář [15] in the case of γ cascades and generalized to coupled $n/\gamma/e^-$ emission by Régnier *et al.* [16]. NR corresponds to the complete level schemes and the associated partial widths of transitions for all nuclei involved in the decay from the primary FF to the fission product. The partial widths follow a statistical χ^2 distribution to account for Porter-Thomas fluctuations [26].

In a FIFRELIN calculation, the level schemes are separated into three regions:

- Below a cut-off energy $E_{\text{cutoff}}(A, Z)$ provided by RIPL-3 [18], the scheme is considered as complete, so only levels from RIPL-3 are considered. When available, ICCs are taken from RIPL, too.
- Above E_{cutoff}, as the discrete level scheme from RIPL is supposed to be incomplete, it is filled with theoretical levels based on level density models. The cumulative number of levels is then:

$$N_c(E) = N_c(E_{\text{cutoff}}) + \int_{E_{\text{cutoff}}}^{E} \rho(x)\,\mathrm{d}x , \tag{7}$$

  where $\rho(x)$ stands for the excitation-energy dependent nuclear level density.
- When the nuclear level density becomes larger than a threshold value, typically 5×10^4 levels/MeV, the levels are stored in energy bins, where their characteristics are averaged. The scheme above this threshold energy E_{bin} is then no longer discrete, but becomes a continuum.

Different models of nuclear level densities are available in FIFRELIN. In this work, we will only focus on two of them. The first one is the Composite Gilbert-Cameron Model (CGCM) [27]. This phenomenological model consists in a Constant Temperature Model (CTM) at low energy and a Fermi Gas Model (FGM) at high energy. In FIFRELIN, we use the parameterization proposed in RIPL-3 [18]. As this model is a macroscopic model, it supposes the parity equipartition of the excited states and a total angular momentum distribution such as given in Eq. (3), which leads to:

$$\rho(E, J, \pi) = \frac{1}{2} \times P(J) \times \rho_{\text{CGCM}}(E) . \tag{8}$$

On the other hand, the microscopic combinatorial level densities avoid this kind of assumption on total angular momentum and parity distributions of excited states [18,28]. Such level densities were calculated by Goriely *et al.* [29] using Hartree-Fock-Bogoliubov (HFB) calculations with the BSk14 effective Skyrme interaction [30]. These densities are tabulated (total angular momentum, parity, energy) for a large number of nuclei in the RIPL-3 database, together with correction parameters. These parameters, denoted c and p, were introduced to improve the reproduction of the discrete levels and the mean resonance spacing of the nuclei, when these quantities are available [18,29]:

$$\rho_{\text{HFB}}(E, J, \pi) = e^{c\sqrt{E-p}} \times \rho_{\text{tab}}(E - p, J, \pi) , \tag{9}$$

where ρ_{tab} is the tabulated value of the level density from the RIPL-3 database. The main identified issue with the use of these level densities in FIFRELIN is the definition of the cut-off energy, E_{cutoff}. Indeed, the one provided in RIPL comes from a fitting procedure between the CTM model and the discrete level schemes of nuclei [18]. Using the same E_{cutoff} with the HFB+BSk14 microscopic level densities is possible, in principle, but this would give rise to consistency issues. Therefore, a HFB-dependent cut-off energy was defined, corresponding to the last discrete level for which the cumulative number of levels, predicted by the HFB model, is smaller than or equal to the number of levels available in the level scheme.

Both these level density models depend on intrinsic free parameters, adjusted on experimental data (discrete levels and mean resonance spacing) in RIPL-3 [18], and on the cut-off energy. Other models used in the code rely on different parameters, e.g. the photon-strength function or the level-density parameter (a). The impact of these 'implicit' parameters will not be discussed here.

4. Results

The impact of the aforementioned models will now be studied through three FIFRELIN calculations. The first calculation (F-1) is based on the CST spin cut-off model with the CGCM level density. This model is the default one (*standard* calculation). For the second calculation (F-2), the CST model has been replaced by the EDS one. For the third calculation (F-3), the EDS model is used together with the HFB + BSk14 nuclear level density. In all calculations, the Enhanced Generalized Lorentzian (EGLO) is used for E1 photo-strength functions, and the neutron transmission coefficients were calculated from the Koning-Delaroche optical model parameterization [31] using TALYS [32]. The maximum emission time for prompt fission γ-rays is 3 ns, to be consistent with the experimental time window [3].

The impact of the spin cut-off model on the mass-dependent prompt fission γ-ray multiplicity was briefly studied for ^{252}Cf(sf) [3] and for ^{237}Np(n,f) [20]. It turned out that the EDS model was much better suited to reproduce the shape of the experimental $\bar{M}_\gamma(A)$ distribution compared to the CST model, especially in the light-fragment region. However, both calculations were over-estimating the average prompt γ-ray multiplicity. Thus, a rescaling of the calculated $\bar{M}_\gamma(A)$ was required in Ref. [3] for instance. With the EDS model, the average FFs total angular momentum as a function of mass follows a 'saw-tooth' like shape, due

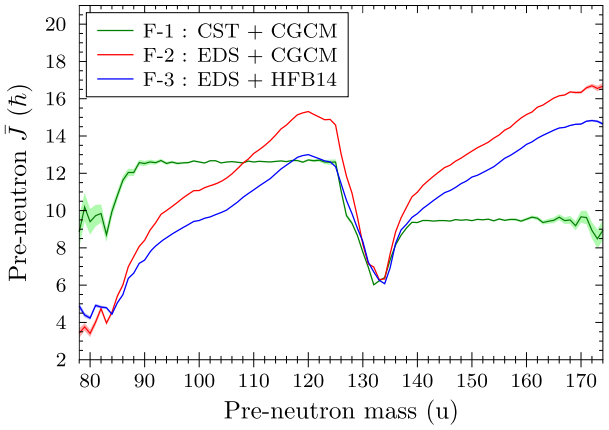

Fig. 2. Average total angular momentum of pre-neutron fission fragments as a function of mass from various FIFRELIN calculations.

Table 1
Free parameters of the FIFRELIN calculations used in this work.

	R_T^{78}	R_T^{132}	k_L / $f_{\sigma,L}$	k_H / $f_{\sigma,H}$
F-1	0.45	1.40	10.5 $\hbar$	8.0 $\hbar$
F-2	0.50	1.40	1.7	1.5
F-3	0.50	1.45	1.4	1.3

Table 2
Average fission fragment angular momentum, before ($\langle J\rangle_{\text{pre}}$) and after ($\langle J\rangle_{\text{post}}$) neutron emission.

	$\langle J_L\rangle_{\text{pre}}$	$\langle J_H\rangle_{\text{pre}}$	$\langle J_L\rangle_{\text{post}}$	$\langle J_H\rangle_{\text{post}}$
F-1	12.61 $\hbar$	9.08 $\hbar$	11.33 $\hbar$	8.28 $\hbar$
F-2	12.66 $\hbar$	11.82 $\hbar$	11.05 $\hbar$	10.26 $\hbar$
F-3	10.79 $\hbar$	10.57 $\hbar$	9.62 $\hbar$	9.39 $\hbar$

to the energy dependence of the spin cut-off, in contrast with the constant behavior imposed by the CST model, as shown in Fig. 2. In this and the following figures, the statistical uncertainties from FIFRELIN calculations are represented in shaded areas.

As discussed in the previous section, each of the FIFRELIN calculations has four free parameters, which were selected to reproduce the average neutron multiplicities, $\bar{\nu}_L = 2.06$ and $\bar{\nu}_H = 1.70$, taken from Ref. [22]. The values of these parameters for each calculation are given in Table 1. In this table, it can be noted that we used a higher spin cut-off for light fragments than for heavy ones, leading to $\bar{J}_L > \bar{J}_H$ (see also Fig. 2 and Table 2). This is consistent with recent theoretical approaches, which revealed that at least for low energy fission light fragments have a higher spin than heavy ones on average [33].

We compare in Fig. 3 the mass-dependent neutron multiplicity distribution, $\bar{\nu}(A)$, from Ref. [5] to the ones obtained with FIFRELIN. We note that all three FIFRELIN calculations give very similar results. Once the free parameters are tuned to best reproduce the average neutron multiplicities, all three models reproduce well the experimentally observed saw-tooth shape of $\bar{\nu}(A)$. This good agreement between the experimental data and the calculations was already discussed in Ref. [1].

In Fig. 4 $\bar{M}_\gamma(A)$ data from ^{252}Cf(sf) [3] are shown together with our three different calculations, F-1 (CST + CGCM), F-2 (EDS + CGCM) and F-3 (EDS + HFB14), respectively, without any rescaling.

The introduction in FIFRELIN of nuclear level densities obtained from HFB+BSk14 calculations enables us to reproduce both the mass-dependent neutron multiplicity $\bar{\nu}(A)$ and the prompt γ-ray multiplicity $\bar{M}_\gamma(A)$, in a consistent calculation (i.e. using a single set of four parameters), for the first time. The numerical results are summarized in Table 3. For the sake of completeness, we mention

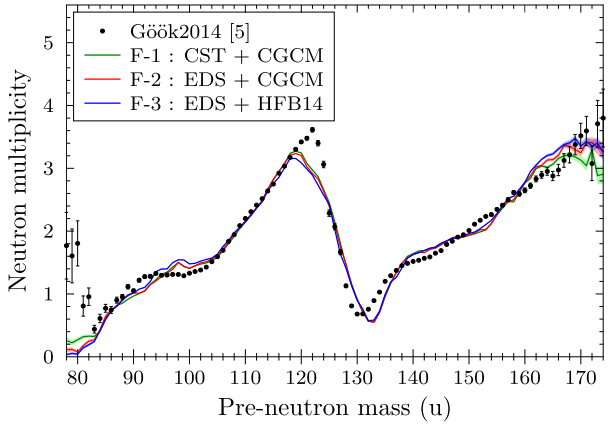

Fig. 3. Prompt neutron multiplicity as a function of fission fragment mass from various FIFRELIN calculations, compared to experimental data [5].

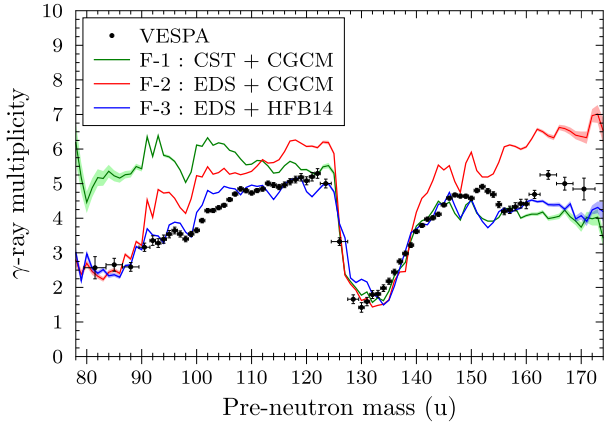

Fig. 4. Prompt fission γ-ray multiplicity as a function of pre-neutron mass for ^{252}Cf(sf) from FIFRELIN calculations, compared to the VESPA data [3].

Table 3
Average prompt fission γ-ray multiplicities obtained with FIFRELIN calculations and VESPA.

	$\bar{M}_{\gamma,tot}$	$\bar{M}_{\gamma,L}$	$\bar{M}_{\gamma,H}$
F-1	9.39 ± 0.05	5.72 ± 0.04	3.67 ± 0.03
F-2	9.79 ± 0.04	5.38 ± 0.04	4.41 ± 0.03
F-3	8.36 ± 0.04	4.67 ± 0.03	3.69 ± 0.02
VESPA	8.37 ± 0.03	4.56 ± 0.03	3.82 ± 0.03

here that calculations using HFB+D1M level densities [34] were also performed. However, the results were not satisfactory and will not be presented here. This might be explained by the slightly better reproduction of experimental neutron spacing resonance by the HFB+BSk14 calculations [34]. This is still under investigation.

As the γ-ray multiplicity as a function of TKE was also measured in Ref. [3], we confronted the FIFRELIN calculations of type F-3 to this experimental data. The results are depicted in Fig. 5. In this figure, some deviations can be observed for the calculated total γ multiplicity as a function of TKE, with respect to the experimental data. First, there is an overestimation of the calculated $\bar{M}_\gamma$(TKE) for TKE $\lesssim$ 180 MeV. The calculation also presents a dip for TKE values between 200 and 210 MeV, which does not appear in the VESPA data. In order to better understand this behavior, we separated $\bar{M}_\gamma$(TKE) for light (L) and heavy (H) fragments, as depicted in Fig. 5. It appears that both the experimental data and the calculation show a rather flat distribution as a function of TKE for the light fragments. We observe that the low-energy overestimation seems to be caused by the light fragments, while the dip

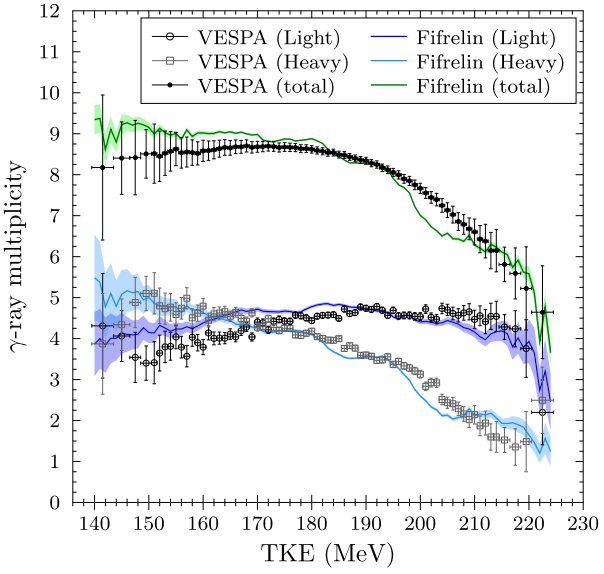

Fig. 5. Prompt fission γ-ray multiplicity distribution as a function of pre-neutron TKE for ^{252}Cf(sf), given separately for light and heavy fragments, and for all fragments [3]. The FIFRELIN calculations were performed within the F-3 model (see text for details).

around 200 MeV comes from the heavy ones. We can also see another dip in the heavy fragments around 185 MeV, which is partially compensated by a slight overestimation of the γ multiplicity from the light fragments at these energies. A similar compensation also occurs at high TKE (above 210 MeV), where the γ multiplicity is overestimated for the heavy fragments, and underestimated for the light ones. The two dips in the calculated TKE-dependent γ multiplicity from the heavy fragments are most likely due to the neutron emission around $\langle S_n \rangle$ and $\langle S_{2n} \rangle$. Indeed, such structures also appear in the TKE-dependent neutron multiplicity distribution, as discussed in Ref. [35].

5. Discussion

The interesting feature from the $\bar{M}_\gamma$(TKE) distributions is the shape difference between light and heavy fragments. For the latter we observe a decrease of the multiplicity with the TKE, whereas for the light fragment an almost flat behavior is observed, in both experiment and calculation. Actually, both the neutron and the γ-ray emissions depend on the available excitation energy of the fragments. More exactly, the γ multiplicity is sensitive to the initial angular momentum, which in the case of the EDS model is linked to the excitation energy. Even if the observed γ emission occurs after neutron emission, the angular momentum taken away from neutrons is small, i.e., about 2.2$\hbar$ per fission for ^{252}Cf(sf). In FIFRELIN, this result comes from the neutron transmission coefficients, which favors low angular momenta. In other words, the higher the angular momentum is, the larger is the number of γ rays necessary to dissipate such angular momentum and to reach the ground state. However, the correlation between TKE and the available excitation energy is not obvious, because all the fragmentations are considered in Fig. 5. Furthermore, the fission process makes the mass split and the TKE correlated. Indeed, the further away from a symmetric mass split the lower is the TKE (see e.g., Ref. [5]). In FIFRELIN, this mechanism is driven by the temperature-ratio parameterization, as depicted in Fig. 1. We found out that this temperature ratio (T_L/T_H) increases with TKE (decreases with TXE). This is linked to the more important increase of the heavy-fragment temperature, (T_H), compared to T_L. This would explain to first order, why the slope of the average γ multiplicity as a function of TKE is stronger for the heavy fragments than for the light ones. Therefore, such behavior from light and heavy fragments is a direct consequence of the energy-sharing process between the two fission fragments, which depends on the temperature of the two nascent fragments at scission. A similar trend is observed for the prompt neutron multiplicity distribution as a function of TKE [19].

6. Conclusion

The new version of the FIFRELIN Monte-Carlo code simultaneously reproduces mass-dependent neutron and γ-ray multiplicity distributions, here demonstrated on the spontaneous fission of ^{252}Cf. This achievement was made possible by using an energy-dependent spin-cutoff model together with combinatorial microscopic HFB+BSk14 nuclear level densities.

In the TKE-dependent γ-multiplicity distribution we observe interesting differences between the light and heavy fragments. The FIFRELIN code describes well the experimental data, even though local deviations for heavy fragments still appear. FIFRELIN has now reached the maturity to investigate the cause of the local differences between calculations and experiment.

Declaration of competing interest

The authors declare that they have no known competing financial interests or personal relationships that could have appeared to influence the work reported in this paper.

Data availability

Data will be made available on request.

References

[1] O. Litaize, O. Serot, L. Berge, Fission modelling with FIFRELIN, Eur. Phys. J. A 51 (12) (2015) 77, https://doi.org/10.1140/epja/i2015-15177-9.
[2] P. Talou, R. Vogt, J. Randrup, et al., Correlated prompt fission data in transport simulations, Eur. Phys. J. A 54 (2018) 9, https://doi.org/10.1140/epja/i2018-12455-0.
[3] M. Travar, V. Piau, A. Göök, O. Litaize, J. Nikolov, A. Oberstedt, S. Oberstedt, J. Enders, M. Peck, W. Geerts, M. Vidali, Experimental information on mass- and TKE-dependence of the prompt fission γ-ray multiplicity, Phys. Lett. B 817 (2021) 136293, https://doi.org/10.1016/j.physletb.2021.136293.
[4] A. Göök, W. Geerts, F.-J. Hambsch, S. Oberstedt, M. Vidali, S. Zeynalov, A position-sensitive twin ionization chamber for fission fragment and prompt neutron correlation experiments, Nucl. Instrum. Methods Phys. Res., Sect. A 830 (2016) 366–374, https://doi.org/10.1016/j.nima.2016.06.002.
[5] A. Göök, F.-J. Hambsch, M. Vidali, Prompt neutron multiplicity in correlation with fragments from spontaneous fission of ^{252}Cf, Phys. Rev. C 90 (2014) 064611, https://doi.org/10.1103/PhysRevC.90.064611.
[6] A. Göök, F.-J. Hambsch, S. Oberstedt, M. Vidali, Prompt neutrons in correlation with fission fragments from ^{235}U(n, f), Phys. Rev. C 98 (2018) 044615, https://doi.org/10.1103/PhysRevC.98.044615.
[7] A. Al-Adili, D. Tarrío, K. Jansson, V. Rakopoulos, A. Solders, S. Pomp, A. Göök, F.-J. Hambsch, S. Oberstedt, M. Vidali, Prompt fission neutron yields in thermal fission of ^{235}U and spontaneous fission of ^{252}Cf, Phys. Rev. C 102 (2020) 064610, https://doi.org/10.1103/PhysRevC.102.064610.
[8] F. Gönnenwein, The Nuclear Fission Process, C. Wagemans Edition, CRC Press, 1991, p. 287, Ch. 8.
[9] A. Oberstedt, R. Billnert, S. Oberstedt, Neutron measurements with lanthanum-bromide scintillation detectors - a first approach, Nucl. Instrum. Methods Phys. Res., Sect. A 708 (2013) 7–14, https://doi.org/10.1016/j.nima.2013.01.005.
[10] H. Maier-Leibnitz, H.W. Schmitt, P. Armbruster, Average number and energy of gamma-rays emitted as a function of fragment mass in U235 thermal-neutron-induced fission, in: Proceedings of the Symposium on Physics and Chemistry of Fission, vol. 2, IAEA, 1965, p. 143.
[11] F. Pleasonton, R.L. Ferguson, H.W. Schmitt, Prompt gamma rays emitted in the thermal-neutron-induced fission of ^{235}U, Phys. Rev. C 6 (1972) 1023–1039, https://doi.org/10.1103/PhysRevC.6.1023.
[12] A. Almazán, L. Bernard, A. Blanchet, A. Bonhomme, et al., Improved STEREO simulation with a new gamma ray spectrum of excited gadolinium isotopes using FIFRELIN, Eur. Phys. J. A 55 (2019) 183, https://doi.org/10.1140/epja/i2019-12886-y.

[13] A.C. Wahl, Nuclear-charge distribution and delayed-neutron yields for thermal-neutron-induced fission of 235U, 233U, and 239Pu and for spontaneous fission of 252Cf, At. Data Nucl. Data Tables 39 (1) (1988) 1–156, https://doi.org/10.1016/0092-640X(88)90016-2.
[14] W. Hauser, H. Feshbach, The inelastic scattering of neutrons, Phys. Rev. 87 (1952) 366–373, https://doi.org/10.1103/PhysRev.87.366.
[15] F. Bečvář, Simulation of γ cascades in complex nuclei with emphasis on assessment of uncertainties of cascade-related quantities, Nucl. Instrum. Methods Phys. Res., Sect. A 417 (2) (1998) 434–449, https://doi.org/10.1016/S0168-9002(98)00787-6.
[16] D. Regnier, O. Litaize, O. Serot, An improved numerical method to compute neutron/gamma deexcitation cascades starting from a high spin state, Comput. Phys. Commun. 201 (2016) 19–28, https://doi.org/10.1016/j.cpc.2015.12.007.
[17] A.V. Ignatyuk, G.N. Smirenkin, A.S. Tishin, Phenomenological description of energy dependence of the level density parameter, Yad. Fiz. 21 (1975) 485–490.
[18] R. Capote, et al., RIPL - reference input parameter library for calculation of nuclear reactions and nuclear data evaluations, Nucl. Data Sheets 110 (12) (2009) 3107–3214, https://doi.org/10.1016/j.nds.2009.10.004, https://www-nds.iaea.org/RIPL-3/.
[19] O. Litaize, O. Serot, Investigation of phenomenological models for the Monte Carlo simulation of the prompt fission neutron and γ emission, Phys. Rev. C 82 (2010) 054616, https://doi.org/10.1103/PhysRevC.82.054616.
[20] L. Thulliez, O. Litaize, O. Serot, A. Chebboubi, Neutron and γ multiplicities as a function of incident neutron energy for the ^{237}Np(n, f) reaction, Phys. Rev. C 100 (2019) 044616, https://doi.org/10.1103/PhysRevC.100.044616.
[21] L. Thulliez, O. Litaize, O. Serot, Sensitivity studies of spin cut-off models on fission fragment observables, EPJ Web Conf. 111 (2016) 10003, https://doi.org/10.1051/epjconf/201611110003.
[22] A.S. Vorobyev, V.N. Dushin, F.-J. Hambsch, V.A. Jakovlev, V.A. Kalinin, A.B. Laptev, B.F. Petrov, O.A. Shcherbakov, Prompt neutron emission from fragments in spontaneous fission of 244, 248Cm and 252Cf, AIP Conf. Proc. 798 (1) (2005) 255–262, https://doi.org/10.1063/1.2137254.
[23] D. Regnier, O. Litaize, O. Serot, Preliminary results of a full Hauser-Feshbach simulation of the prompt neutron and Gamma emission from fission fragments, in: Scientific Workshop on Nuclear Fission Dynamics and the Emission of Prompt Neutrons and Gamma Rays, Biarritz, France, 28–30 November 2012, Phys. Proc. 47 (2013) 47–52, https://doi.org/10.1016/j.phpro.2013.06.008.
[24] T. Kibédi, T. Burrows, M. Trzhaskovskaya, P. Davidson, C. Nestor, Evaluation of theoretical conversion coefficients using BrIcc, Nucl. Instrum. Methods Phys. Res., Sect. A 589 (2) (2008) 202–229, https://doi.org/10.1016/j.nima.2008.02.051.
[25] A. Chebboubi, Private Communication, 2021.
[26] C.E. Porter, R.G. Thomas, Fluctuations of nuclear reaction widths, Phys. Rev. 104 (1956) 483–491, https://doi.org/10.1103/PhysRev.104.483.
[27] A. Gilbert, A.G.W. Cameron, A composite nuclear-level density formula with shell corrections, Can. J. Phys. 43 (8) (1965) 1446–1496, https://doi.org/10.1139/p65-139.
[28] S. Hilaire, S. Goriely, A.J. Koning, Global microscopic nuclear level densities within the HFB plus combinatorial method for practical applications, in: International Conference on Nuclear Data for Science and Technology, 2007, pp. 199–202.
[29] S. Goriely, S. Hilaire, A.J. Koning, Improved microscopic nuclear level densities within the Hartree-Fock-Bogoliubov plus combinatorial method, Phys. Rev. C 78 (2008) 064307, https://doi.org/10.1103/PhysRevC.78.064307.
[30] S. Goriely, M. Samyn, J.M. Pearson, Further explorations of Skyrme-Hartree-Fock-Bogoliubov mass formulas. VII. Simultaneous fits to masses and fission barriers, Phys. Rev. C 75 (2007) 064312, https://doi.org/10.1103/PhysRevC.75.064312.
[31] A.J. Koning, J.P. Delaroche, Local and global nucleon optical models from 1 kev to 200 MeV, Nucl. Phys. A 713 (3) (2003) 231–310, https://doi.org/10.1016/S0375-9474(02)01321-0.
[32] A.J. Koning, S. Hilaire, S. Goriely, https://tendl.web.psi.ch/tendl_2019/talys.html.
[33] P. Marević, N. Schunck, J. Randrup, R. Vogt, Angular momentum of fission fragments from microscopic theory, Phys. Rev. C 104 (2) (2021) L021601, https://doi.org/10.1103/PhysRevC.104.L021601.
[34] S. Hilaire, M. Girod, S. Goriely, A.J. Koning, Temperature-dependent combinatorial level densities with the D1M Gogny force, Phys. Rev. C 86 (6) (2012) 064317, https://doi.org/10.1103/PhysRevC.86.064317.
[35] O. Litaize, O. Serot, L. Thulliez, A. Chebboubi, Prompt particle emission in correlation with fission fragments, EPJ Web Conf. 146 (2017) 04006, https://doi.org/10.1051/epjconf/201714604006.